Research Article Vol. 33, No. 7 / 7 Apr 2025 / Optics Express 15057
Optics EXPRESS

Spectroscopy and SESAM mode-locking of a disordered Yb:$Gd_2SrAl_2O_7$ crystal

HUANG-JUN ZENG,[1,2] ZHANG-LANG LIN,[1] PAVEL LOIKO,[3] FEIFEI YUAN,[1] GE ZHANG,[1] ZHOUBIN LIN,[1] XAVIER MATEOS,[4] VALENTIN PETROV,[5] AND WEIDONG CHEN[1,5,*]

[1]*State Key Laboratory of Functional Crystals and Devices, Fujian Institute of Research on the Structure of Matter, Chinese Academy of Sciences, 350002 Fuzhou, China*
[2]*University of Chinese Academy of Science, Beijing 100049, China*
[3]*Centre de Recherche sur les Ions, les Matériaux et la Photonique (CIMAP), UMR 6252 CEA-CNRS-ENSICAEN, Université de Caen, 6 Boulevard Maréchal Juin, 14050 Caen Cedex 4, France*
[4]*Universitat Rovira i Virgili, URV, Física i Cristal·lografia de Materials, (FiCMA)- Marcel·lí Domingo 1, 43007 Tarragona, Spain*
[5]*Max Born Institute for Nonlinear Optics and Short Pulse Spectroscopy, Max-Born-Str. 2a, 12489 Berlin, Germany*
[*]*chenweidong@fjirsm.ac.cn*

Abstract: We report on the polarized spectroscopy, continuous-wave laser operation, and mode-locked laser performance of an ytterbium-doped disordered tetragonal rare-earth strontium aluminate crystal, Yb^{3+}:$Gd_2SrAl_2O_7$. In the continuous-wave regime, the diode-pumped Yb:$Gd_2SrAl_2O_7$ laser generated a maximum output power of 487 mW at 1064 nm (π-polarization), with a slope efficiency of 61%. By employing a commercial SESAM to initiate and stabilize soliton-like pulse formation, the mode-locked Yb:$Gd_2SrAl_2O_7$ laser generated transform-limited pulses as short as 38 fs at 1065.7 nm, with an average output power of 87 mW at a repetition rate of ~66.5 MHz. The average output power was further scaled to 131 mW for slightly longer pulse duration of 43 fs, corresponding to a peak power of 40.3 kW and a laser efficiency of 15.5%. To the best of our knowledge, this is the first demonstration of mode-locked laser operation of the Yb:$Gd_2SrAl_2O_7$ crystal.

1. Introduction

Ytterbium (Yb^{3+}) doped, structurally disordered laser crystals with relatively high thermal conductivity and broad, flat and smooth gain profiles are highly promising for the development of high-power, femtosecond lasers via passive mode-locking [1,2]. One well-known example is the family of Yb^{3+}-doped calcium rare-earth aluminate (Yb:Ca*RE*AlO_4) crystals, where RE^{3+} represents Gd^{3+} or Y^{3+}, such as Yb:$CaGdAlO_4$ (Yb:CALGO) and Yb:$CaYAlO_4$ (Yb:CALYO). These crystals exhibit "glassy-like" spectral behavior while maintaining excellent thermo-optic and thermal properties [3,4], making them highly suitable for power-scalable, sub-100 fs, mode-locked (ML) laser operation in the ~1 μm spectral range [5–7]. In combination with Kerr-lens mode-locking (KLM), oscillators based on Yb:Ca*RE*AlO_4 crystals have directly generated sub-30 fs [8–10] and even sub-20 fs pulses [11,12].

Yb^{3+}-doped gadolinium strontium double aluminate (Yb:$Gd_2SrAl_2O_7$, abbreviated as Yb:SALGO) belongs to another family of disordered rare-earth aluminate crystals. It crystallizes in the pseudobinary Gd_2O_3 – $SrAl_2O_4$ system and belongs to the Ruddlesden – Popper phase, characterized by an alternating block structure formed by perovskite (P) and rock salt (RS) layers [13]. Yb:SALGO exhibits a tetragonal symmetry (sp. gr. *I*4/*mmm*, $Sr_3Ti_2O_7$ structural type) and is an optically uniaxial crystal. Thanks to its relatively low melting point of 1780°C and congruent melting character, growth in large volumes is possible by the Czochralski method.

#559152 https://doi.org/10.1364/OE.559152
Journal © 2025 Received 19 Feb 2025; revised 13 Mar 2025; accepted 14 Mar 2025; published 25 Mar 2025

Optics EXPRESS

The structural disorder in SALGO originates from the random occupation of two non-equivalent lattice sites in the P and RS layers by the Gd^{3+} and Sr^{2+} cations. As a result, Yb^{3+} dopant ions in the SALGO crystal experience significant local crystal field variations, leading to substantial inhomogeneous spectral line broadening and "glassy-like" spectroscopic behavior, with broad absorption and emission bands [14]. The broadband emission is particularly favorable for generating ultrashort (sub-50 fs) pulses via passive mode-locking. Yb:SALGO also exhibits reasonably high thermal conductivity (4.84 $Wm^{-1}K^{-1}$ at room temperature, RT) [14], making it suitable for power-scalable operation. Indeed, a continuous-wave (CW) Yb:SALGO laser pumped by a spatially multimode fiber-coupled InGaAs laser diode generated 7.35 W of output power at ~1066 nm, with a reasonably high slope efficiency of 53.7% [14].

The combination of broadband spectral gain, good thermal properties, and moderate luminescence lifetime (0.358 ms in powder samples eliminating the reabsorption effect) makes Yb:SALGO an attractive candidate for developing high-power tunable and femtosecond lasers and amplifiers operating in the ~1 μm spectral range when pumped by commercially available InGaAs laser diodes at ~980 nm. The relatively large Stark splitting of the Yb^{3+} ground-state ($^2F_{7/2}$) manifold (747 cm^{-1}) in SALGO facilitates low-threshold laser operation. Additionally, the relatively broad zero-phonon line (ZPL) with a full width at half maximum (FWHM) of 23 nm at 981.2 nm for π-polarization ($\boldsymbol{E} \parallel \boldsymbol{c}$) at room temperature, relaxes the requirements for precise wavelength stabilization of high-power InGaAs pump lasers.

In this work, we study the polarized spectroscopy of Yb:SALGO. Using a commercial SESAM as a saturable absorber (SA), we demonstrate passively ML operation of a diode-pumped Yb:SALGO laser for the first time, generating sub-40 fs soliton pulses.

2. Optical spectroscopy

The factor group analysis for the primitive cell of the D_{4h}^{17} symmetry predicts the following set of irreducible representations at the center of the Brillouin zone ($\boldsymbol{k} = 0$): $\Gamma = 2A_{1g} + 2E_g + 4A_{2u} + 5E_u + B_{2u}$ [15,16]. Among these, the Raman-active modes ($2A_{1g} + 2E_g$) belong to even-parity species and primarily involve the vibrations of specific atomic groups, particularly Sr/Gd and O atoms. Specifically, the $A_{1g} + E_g$ modes associated with Sr/Gd vibrations appear at 195 cm^{-1} and 225 cm^{-1}, while those related to O vibrations contribute to the high-frequency band, exhibiting a complex structure. The remaining vibrational modes are classified as follows: infrared (IR)-active modes ($3A_{2u} + 4E_u$), acoustic modes ($A_{2u} + E_u$), and silent modes (B_{2u}) [16]. The polarized Raman spectra of an ***a***-cut Yb:SALGO crystal in $a(ij)\bar{a}$ geometries using Porto's notations [17] with i, j denoting the π ($\boldsymbol{E} \parallel \boldsymbol{c}$) and σ ($\boldsymbol{E} \perp \boldsymbol{c}$) polarization, exhibit strong polarization effects, as shown in Fig. 1. All Raman-active modes are clearly observed. In the $a(\pi\pi)\bar{a}$ geometry, the A_{1g} mode appears at 225 cm^{-1}, while in the $a(\pi\sigma)\bar{a}$ geometry, the E_g mode is detected at 195 cm^{-1}. The dominant band at 195/225 cm^{-1} is therefore attributed to Sr/Gd vibrations along the ***c***-axis, whereas the high-frequency band at 637 cm^{-1} is assigned to O vibrations.

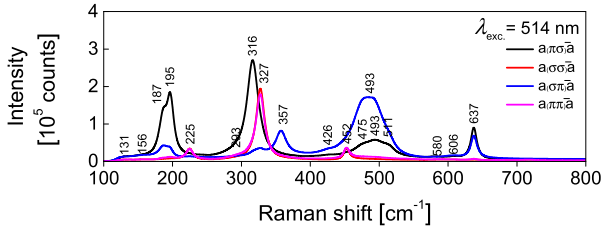

Fig. 1. RT polarized Raman spectra of Yb:SALGO crystal: (a) $a(ij)\bar{a}$, where $i, j = \pi$ ($\boldsymbol{E} \parallel \boldsymbol{c}$) and σ ($\boldsymbol{E} \perp \boldsymbol{c}$) geometries (Porto's notations); $\lambda_{exc} = 514$ nm.

Optics EXPRESS

Figure 2 presents the RT polarized absorption cross-section (σ_{abs}) and stimulated-emission (SE) cross-section (σ_{SE}) spectra of Yb:SALGO, measured for the two principal light polarizations, σ ($\boldsymbol{E} \perp \boldsymbol{c}$) and π ($\boldsymbol{E} \parallel \boldsymbol{c}$). The maximum σ_{abs} for the $^2F_{7/2} \leftrightarrow {}^2F_{5/2}$ transition, corresponding to the ZPL of Yb^{3+}, is 5.31×10^{-20} cm^2 at 981.2 nm, with a FWHM of 23 nm for π-polarization. For σ-polarization, the σ_{abs} peak value is lower, 4.37×10^{-20} cm^2 at 981.3 nm, with a FWHM of 15 nm. The RT σ_{SE} spectra were calculated using a combination of the Füchtbauer–Ladenburg (F-L) formula and the reciprocity method, as shown in Fig. 2 by the blue lines. In the spectral range where laser operation can be expected due to reabsorption, at wavelengths longer than the ZPL, σ_{SE} reaches 1.27×10^{-20}cm^2 at ~1057 nm for σ-polarization, whereas for π-polarization, it is 0.93×10^{-20}cm^2 at ~1066 nm. The inherent anisotropy observed in σ_{SE} suggests that Yb:SALGO lasers based on ***a***-cut crystals are likely to naturally emit linearly polarized light.

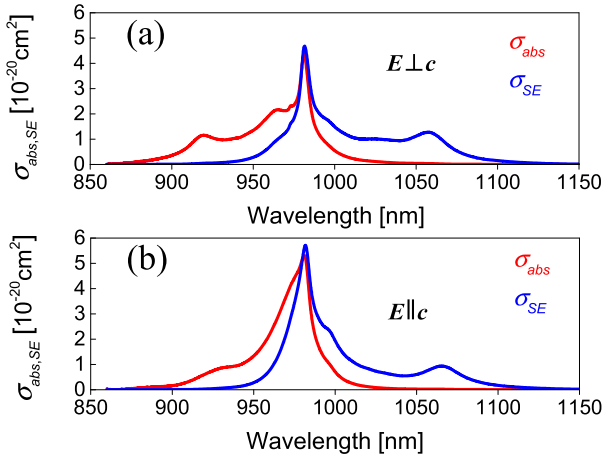

Fig. 2. RT polarized spectroscopy of Yb:SALGO: absorption (σ_{abs}) and stimulated-emission (σ_{SE}) cross-sections for light polarizations (a) $\boldsymbol{E} \perp \boldsymbol{c}$ (σ) and (b) $\boldsymbol{E} \parallel \boldsymbol{c}$ (π).

Figure 3 presents the RT luminescence decay curves measured for both a bulk sample (*blue* color) and a finely powdered sample (*red* color). The decay follows a single-exponential dependence, with a luminescence lifetime ($\tau_{lum.}$) of 529 μs for the bulk sample and 358 μs for the powder. The longer $\tau_{lum.}$ observed in the bulk sample, compared to the powdered one, is attributed to the effect of radiation trapping [18].

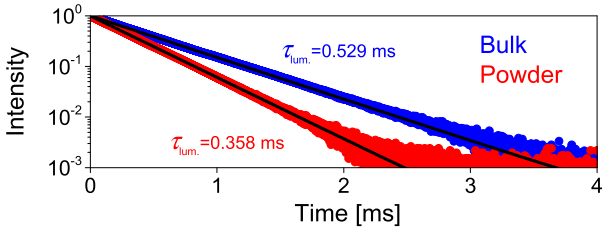

Fig. 3. RT luminescence decay curves of 1.97 at.% Yb:SALGO for bulk (*blue*) and powdered (*red*) samples, $\lambda_{exc} = 978$ nm, $\lambda_{lum} = 1030$ nm, *black lines* – single-exponential fits.

Optics EXPRESS

The polarized gain cross-sections, given by $\sigma_{gain} = \beta\sigma_{SE} - (1 - \beta)\sigma_{abs}$, were obtained for the two principal polarizations, π and σ, based on the quasi-three-level nature of the Yb laser scheme, which inherently includes reabsorption, as illustrated in Fig. 4. Here, $\beta = N_2/N_{Yb}$ is the inversion ratio, where N_2 corresponds to the population of the upper laser level ($^2F_{5/2}$). The local structure and compositional disorder leads to inhomogeneous broadening of the spectral lines, resulting in a "glassy-like" spectroscopic behavior. The gain spectra extend significantly beyond the range of electronic transitions, which can be attributed to substantial phonon sidebands caused by vibronic interactions in Yb:SALGO. As the inversion ratio increases, the spectral peak undergoes a blue-shift, from 1070 nm at $\beta = 0.03$ to 1066 nm at $\beta = 0.18$, the gain bandwidth (FWHM) reaches ~38 nm for π-polarization and ~57 nm for σ-polarization. The broad gain spectrum of Yb:SALGO highlights its potential for wide wavelength tuning and generation of sub-50 fs pulses from ML lasers.

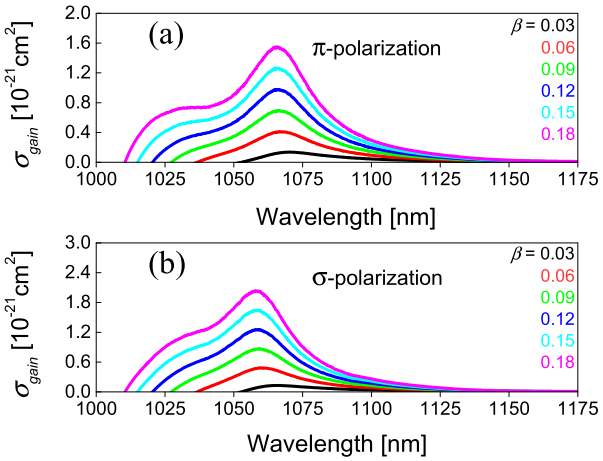

Fig. 4. RT polarized gain cross-section (σ_{gain}) spectra of Yb:SALGO, $\sigma_{gain} = \beta\sigma_{SE} - (1 - \beta)\sigma_{abs}$, $\beta = N_2(^2F_{5/2})/N_{Yb}$ – population inversion ratio. The light polarization is (a) π and (b) σ.

The low-temperature (LT, 12 K) unpolarized absorption and emission spectra of Yb^{3+} in SALGO were measured to analyze the crystal-field splitting, as shown in Fig. 5.

In Yb:SALGO, the host-forming Gd^{3+} and Sr^{2+} cations are statistically distributed across two identical lattice sites, 2*b* and 4*e*, with $D_{4\,h}$ symmetry, and are IX-fold coordinated by oxygen [19]. The $^2F_{7/2}$ and $^2F_{5/2}$ manifolds of the Yb^{3+} ion are split by the crystal field into four and three Stark components, respectively, which are labeled in this work as 0–3 ($^2F_{7/2}$) and 0' – 2' ($^2F_{5/2}$). The LT spectra of Yb:SALGO exhibit a significant inhomogeneous spectral line broadening, attributed to the varying composition of the second coordination sphere around the active ions, which consists of both Sr^{2+} and Gd^{3+} cations. For the SALGO host crystal, the Yb^{3+} ZPL (corresponding to the 0↔0' transition) has an energy E_{ZPL} of 10181 cm^{-1}, while the total splitting of the ground state, $\Delta E(^2F_{7/2})$, amounts to 747 cm^{-1}. The experimental crystal-field splitting of the Yb^{3+} levels in this crystal is presented in Fig. 5(c).

Optics EXPRESS

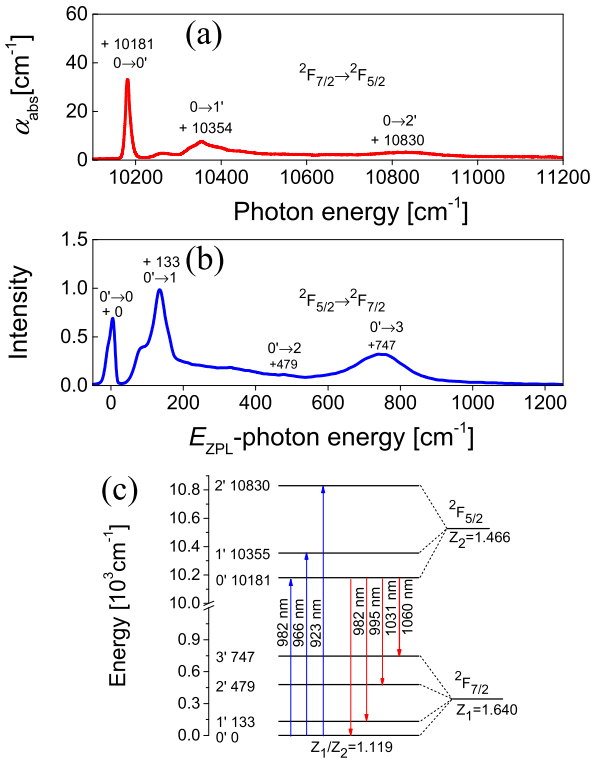

Fig. 5. LT (12 K) (a) absorption and (b) luminescence spectra of Yb:SALGO. "+" mark the electronic transitions; (c) crystal-field splitting for the Yb^{3+} levels in SALGO.

3. Laser set-up

The schematic of the diode-pumped Yb:SALGO laser is shown in Fig. 6. The pump source was a spatially single-mode, fiber-coupled InGaAs laser diode emitting 1.3 W of unpolarized radiation. This laser diode featured a fiber Bragg grating (FBG) for wavelength locking and spectral narrowing, resulting in a spectral linewidth of 0.2 nm (FWHM) at 976 nm. The nearly diffraction-limited pump beam (beam propagation factor, $M^2 = 1.02$) was collimated by an aspherical lens L_1 (focal length, $f = 26$ mm) and then focused into the crystal using a spherical lens L_2 ($f = 75$ mm). This arrangement yielded a beam waist (radius) of 16 µm × 35 µm in the sagittal and tangential planes, respectively.

The laser crystal was an ***a***-cut Yb:SALGO with an actual doping level of 1.97 at.%. The sample had an aperture of 3 mm × 3 mm and a thickness of 3 mm. Both surfaces were polished to laser grade but remained uncoated. The crystal was mounted in a copper holder without active cooling and positioned at Brewster's angle between two plane-concave mirrors, M_1 and M_2 (radius of curvature, RoC = −100 mm), in an X-folded, astigmatically compensated standing wave cavity to minimize optical losses at the laser wavelength. The Brewster angle was adjusted to support π-polarization for maximized pump absorption efficiency in the ZPL although the Yb:SALGO gain cross-section for this polarization is lower.

The CW laser performance of the Yb:SALGO crystal was investigated using a simplified four-mirror cavity without the SASAM and the dispersive mirrors (DMs). One cavity arm was terminated by a flat rear mirror M_3, while the other ended with a plane-wedged output coupler (OC) providing variable transmission at the laser wavelength (T_{OC}) in the range of 0.6% to 7.5%. The cavity mode size in the laser crystal was calculated using the ray transfer matrix formalism,

Optics EXPRESS

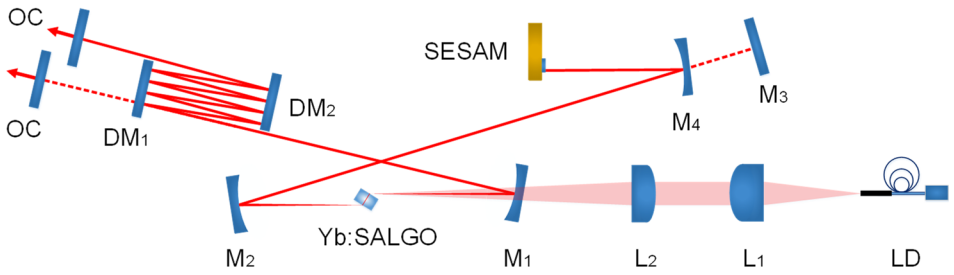

Fig. 6. Schematic of the diode-pumped Yb:SALGO laser. LD: fiber-coupled laser diode; L_1: aspherical lens; L_2: spherical lens; M_1, M_2 and M_4: plane-concave mirrors (RoC = −100 mm); M_3: flat rear mirror; DM_1 and DM_2: flat dispersive mirrors; OC: plane-wedged output coupler; SESAM: SEmiconductor Saturable Absorber Mirror.

yielding a beam waist (radius) of 21 µm × 40 µm in the sagittal and tangential planes, respectively. This method enabled precise determination of the beam size, optimizing the overlap between the laser mode and the gain region within the crystal. Under lasing conditions, the measured pump absorption varied slightly with T_{OC}, from 68% to 70%.

In the ML regime, the flat rear mirror M_3 was replaced with a third plane-concave mirror M_4 (RoC = −100 mm), forming a secondary intracavity beam waist with a radius of ~80 µm at the SESAM, to ensure its efficient bleaching. The SESAM, used as a rear reflector, was a commercial device (BATOP, GmbH) with a modulation depth of ~0.6% at ~1 µm, a non-saturable loss of ~0.4%, a saturation fluence of 70 µJ/cm^2, and a recovery time of ~1 ps. In the extended cavity arm, two flat DMs (DM_1 and DM_2) were implemented to manage the intracavity group delay dispersion (GDD), each providing a GDD of −100 fs^2 per bounce. This configuration introduced a total round-trip negative GDD of −1600 fs^2, effectively compensating for the material dispersion of the laser crystal and balancing the self-phase modulation (SPM) induced by the Kerr nonlinearity of the gain medium. The geometric cavity length of the ML laser was ~2 m, resulting in a pulse repetition rate of ~66.5 MHz.

4. Laser performance

4.1. Continuous-wave laser operation

The CW laser performance of the Yb:SALGO laser is illustrated in Fig. 7. A maximum output power of 487 mW was achieved at 1064 nm using a 4% OC at an absorbed pump power of 931 mW, corresponding to a laser efficiency (η_{laser}) of 52.3% and a slope efficiency (η) of 61.0%, as shown in Fig. 7(a). The laser threshold increased with T_{OC}, from 45 mW (T_{OC} = 0.6%) to 197 mW (T_{OC} = 7.5%). A slight blue-shift in the laser wavelength was observed in the CW regime as T_{OC} increased, from 1072 to 1063 nm, as shown in Fig. 7(b). This behavior is characteristic of quasi-three-level Yb lasers, where reabsorption at the laser wavelength plays a role, and is consistent with the gain spectra of Yb:SALGO shown in Fig. 4.

Figure 8(a) presents a Caird analysis, used to estimate the passive losses of the diode-pumped Yb:SALGO laser in the CW regime. The measured slope efficiency η was fitted as a function of –ln(R_{OC}), where $R_{OC} = 1 - T_{OC}$ represents the OC reflectivity [20]. This analysis yielded total round-trip cavity losses of $\delta = 0.7 \pm 0.14\%$ (reabsorption losses excluded) and an intrinsic slope efficiency of $\eta_0 = 75.5 \pm 1\%$.

To investigate the wavelength tuning capability of the diode-pumped CW Yb:SALGO laser, a quartz-based Lyot filter was inserted at Brewster's angle near the OC. Using a 1% OC and an incident pump power of 800 mW, a broad wavelength tuning range of 86 nm was achieved, spanning from 1019 to 1105 nm.

Optics EXPRESS

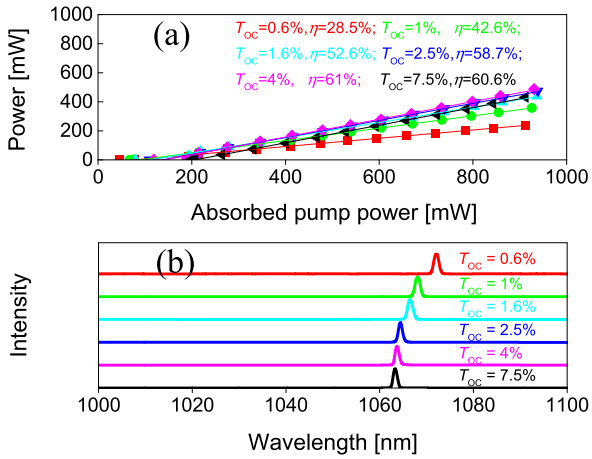

Fig. 7. Diode-pumped CW Yb:SALGO laser: (a) input - output dependences for different OCs, η – slope efficiency; (b) laser emission spectra (π-polarization).

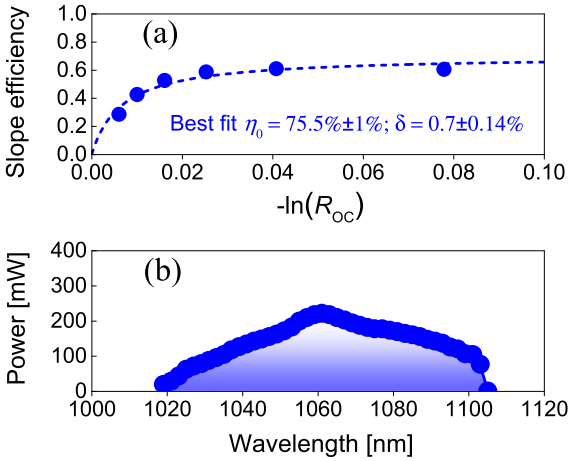

Fig. 8. Diode-pumped CW Yb:SALGO laser: (a) Caird analysis: laser slope efficiency plotted *vs.* –ln(R_{OC}); (b) laser tuning curve obtained with a 1% OC and a quartz-based Lyot filter.

4.2. *Mode-locked laser operation*

ML operation was initiated and stabilized using a commercial SESAM. Soliton-like pulse shaping using a 2.5% OC was realized for the total negative GDD of −1600 fs^2 and resulted in stable and self-starting ML operation.

The spectral and temporal characteristics of the diode-pumped ML Yb:SALGO laser are presented in Fig. 9. The Yb:SALGO laser generated soliton pulses centered at 1065.3 nm with a spectral bandwidth of 28.3 nm (FWHM), assuming a sech^2 spectral shape, as shown in Fig. 9(a). The recorded second-harmonic generation (SHG)-based intensity autocorrelation trace was well fitted with a sech^2-shaped temporal profile, yielding an estimated pulse duration of 43 fs (FWHM), as depicted in Fig. 9(b). The corresponding time-bandwidth product (TBP) was calculated to be 0.321, close to the value for Fourier-transform-limited pulses (0.315). A long-range (50 ps) SHG-based intensity autocorrelation scan confirmed the steady-state, single-pulse mode-locking operation, as shown in the inset of Fig. 9(b). The maximum average output power was 131 mW

Optics EXPRESS

at an absorbed pump power of 0.847 W, corresponding to a laser efficiency of 15.5% and a peak power of 40.3 kW.

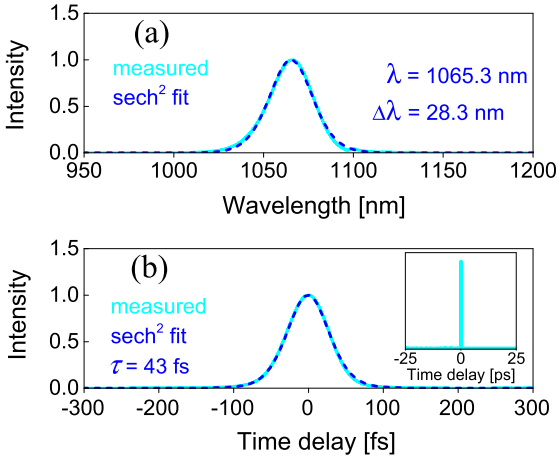

Fig. 9. Diode-pumped ML Yb:SALGO laser with $T_{OC} = 2.5\%$. (a) Optical spectrum; (b) SHG-based intensity autocorrelation trace, *dashed curves* - sech^2 fits. *Inset*: intensity autocorrelation trace measured on a time span of 50 ps.

The shortest pulses with optimal stability were obtained using a 1.6% OC. The measured laser spectrum is shown in Fig. 10(a). Assuming a sech^2-shaped spectral profile, the Yb:SALGO laser delivered soliton pulses with a spectral bandwidth of 31.5 nm (FWHM) at a central wavelength of 1065.7 nm. The pulse duration was estimated from the SHG-based intensity autocorrelation trace, as shown in Fig. 10(b). The curve was well fitted with a sech^2-shaped temporal profile, yielding an estimated pulse duration of 38 fs (FWHM). The corresponding TBP was 0.316, almost equal to the Fourier-transform-limited value. The inset of Fig. 10(b) presents the SHG-based intensity autocorrelation trace over a long-time span of 50 ps, confirming stable single-pulse CW ML operation free from multiple-pulse instabilities. The average output power for the shortest pulses

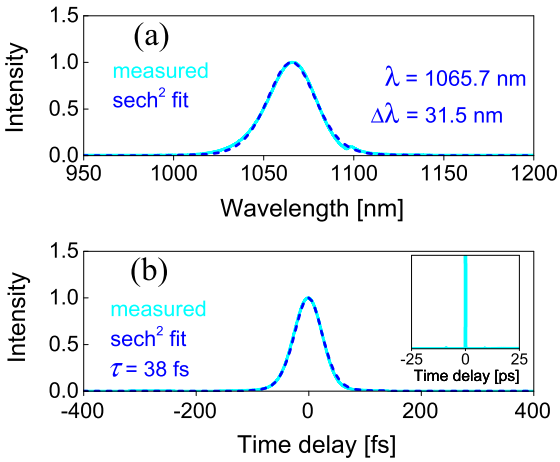

Fig. 10. Diode-pumped ML Yb:SALGO laser with $T_{OC} = 1.6\%$. (a) Optical spectrum; (b) SHG-based intensity autocorrelation trace, *dashed curves* - sech^2 fits. *Inset*: intensity autocorrelation trace measured on a time span of 50 ps.

Optics EXPRESS

was 87 mW at an absorbed pump power of 883 mW, corresponding to a laser efficiency of 9.9% and a peak power of 30.3 kW. The measured beam propagation factor (M^2) of the shortest pulses was 1.02.

To further verify the stability of the ML operation for the shortest pulses, a radio-frequency (RF) spectrum analyzer was used to record the beat note in different frequency ranges. The fundamental beat note at 66.51 MHz exhibited a high extinction ratio of >76 dBc above the carrier, cf. Figure 11(a). Additionally, the uniform harmonics recorded over a 1-GHz frequency span provided strong evidence of highly stable CW ML operation, free from any Q-switching or multi-pulsing instabilities, as shown in Fig. 11(b).

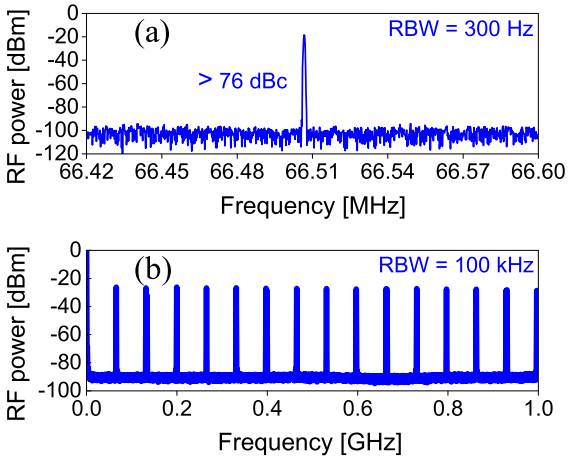

Fig. 11. RF spectra of the diode-pumped ML Yb:SALGO laser with $T_{OC} = 1.6\%$: (a) fundamental beat note at 66.51 MHz recorded with a resolution bandwidth (RBW) of 300 Hz, and (b) harmonics on a 1-GHz frequency span recorded with a RBW of 100 kHz.

5. Conclusion

In conclusion, this work presents the spectroscopic characterization and the first demonstration of passively mode-locked laser operation using the disordered Yb:SALGO crystal. The "glassy-like" spectroscopic properties of Yb:SALGO highlight its potential for ultrashort pulse generation in a mode-locked lasers. In CW operation regime, the diode-pumped Yb:SALGO laser generated a maximum output power of 487 mW at 1064 nm, with a slope efficiency of 61% and a laser efficiency of 52.3%. A broad wavelength tuning range from 1019 to 1105 nm (spanning across 86 nm) was realized using a Lyot filter. Under mode-locked operation, the diode-pumped Yb:SALGO laser delivered soliton pulses as short as 38 fs at 1065.7 nm, with an average output power of 87 mW and a pulse repetition rate of 66.51 MHz. Mode-locking was initiated and stabilized using a commercial SESAM. Further pulse shortening and power scaling could be achieved through soft-aperture Kerr-lens mode-locking.

Funding. National Natural Science Foundation of China (62475263); Project of Science and Technology of Fujian Province (2024I0041, 2023H0047, 2023H0042); Sino-German Scientist Cooperation and Exchanges Mobility Program (M-0040); Ministerio de Ciencia, Innovación y Universidades (PID2022-141499OB-I00).

Acknowledgment. Xavier Mateos acknowledges the Serra Húnter program.

Disclosures. The authors declare no conflicts of interest.

Data availability. Data underlying the results presented in this paper are not publicly available at this time but may be obtained from the authors upon reasonable request.

Optics EXPRESS

References

1. Z. L. Lin, H. J. Zeng, Z. Pan, *et al.*, "Kerr-lens mode-locking of an Yb:SALLO laser generating 25 fs pulses at 1090 nm," Appl. Phys. Lett. **124**(17), 171102 (2024).
2. Z. L. Lin, P. Loiko, H. J. Zeng, *et al.*, "Kerr-lens mode-locking of an Yb:CLNGG laser," Opt. Express **31**(5), 8575–8585 (2023).
3. P. Loiko, J. M. Serres, X. Mateos, *et al.*, "Microchip Yb:$CaLnAlO_4$ lasers with up to 91% slope efficiency," Opt. Lett. **42**(13), 2431–2434 (2017).
4. P. Loiko, F. Druon, P. Georges, *et al.*, "Thermo-optic characterization of Yb:$CaGdAlO_4$ laser crystal," Opt. Mater. Express **4**(11), 2241–2249 (2014).
5. W. Tian, X. Tian, Q. Li, *et al.*, "Kerr-lens mode-locked femtosecond Yb:CALYO oscillator with more than 20-W average power," Opt. Lett. **48**(18), 4789–4792 (2023).
6. D. Y. Kim, B. J. Park, S. Y. Lee, *et al.*, "High-power 50 fs Kerr-lens mode-locked Yb:CALGO oscillator," Opt. Laser Technol. **159**, 109019 (2023).
7. W. Tian, R. Xu, L. Zheng, *et al.*, "10-W-scale Kerr-lens mode-locked Yb:CALYO laser with sub-100-fs pulses," Opt. Lett. **46**(6), 1297–1300 (2021).
8. F. Trawi, J. Drs, M. Müller, *et al.*, "Sub-30-fs Yb:CALGO laser oscillator based on cross-polarized multi-mode diode pumping," Opt. Express **32**(21), 37897–37905 (2024).
9. F. Labaye, V. J. Wittwer, M. Hamrouni, *et al.*, "Efficient few-cycle Yb-doped laser oscillator with Watt-level average power," Opt. Express **30**(2), 2528–2538 (2022).
10. S. Kimura, S. Tani, and Y. Kobayashi, "Raman-assisted broadband mode-locked laser," Sci. Rep. **9**(1), 3738 (2019).
11. Y. Wang, X. Su, Y. Xie, *et al.*, "17.8 fs broadband Kerr-lens mode-locked Yb:CALGO oscillator," Opt. Lett. **46**(8), 1892–1895 (2021).
12. J. Ma, F. Yang, W. Gao, *et al.*, "Sub-five-optical-cycle pulse generation from a Kerr-lens mode-locked Yb:$CaYAlO_4$ laser," Opt. Lett. **46**(10), 2328–2331 (2021).
13. I. Zvereva, Y. Smirnov, V. Gusarov, *et al.*, "Complex aluminates $RE_2SrAl_2O_7$ (RE = La, Nd, Sm – Ho): Cation ordering and stability of the double perovskite slab–rocksalt layer P_2/RS intergrowth," Solid State Sci. **5**(2), 343–349 (2003).
14. F. Yuan, Y. Huang, L. Liu, *et al.*, "Spectroscopic properties and continuous-wave laser performance of Yb:$Gd_2SrAl_2O_7$ crystal," J. Alloys Compd. **808**, 151715 (2019).
15. D. L. Rousseau, R. P. Bauman, and S. Porto, "Normal mode determination in crystals," J. Raman Spectrosc. **10**(1), 253–290 (1981).
16. V. Hadjiev, M. Cardona, I. Ivanov, *et al.*, "Optical phonons probe of the $SrLaAlO_4$ crystal structure," J. Alloys Compd. **251**(1-2), 7–10 (1997).
17. T. C. Damen, S. Porto, and B. Tell, "Raman effect in zinc oxide," Phys. Rev. **142**(2), 570–574 (1966).
18. D. S. Sumida and T. Y. Fan, "Effect of radiation trapping on fluorescence lifetime and emission cross-section measurements in solid-state laser media," Opt. Lett. **19**(17), 1343–1345 (1994).
19. I. Zvereva, A. Isaeva, and J. Choisnet, "Cation distribution and interatomic interactions in oxides with heterovalent isomorphism: XI.$(La_{1-x}Ho_x)_2SrAl_2O_7$ solid solutions," Russ. J. Gen. Chem. **76**(6), 875–880 (2006).
20. J. A. Caird, S. A. Payne, P. R. Staver, *et al.*, "Quantum electronic properties of the $Na_3Ga_2Li_3F_{12}$: Cr^{3+} laser," IEEE J. Quantum Electron. **24**(6), 1077–1099 (1988).